Image-based Rendering of the Anisotropic BRDF of Woven Fabrics

Yuki Takeda, Huynh Quang Huy Viet and Hiromi T.Tanaka

Computer Vision Laboratory, Department of Human and Computer Intelligence,
College of Information Science & Engineering, Ritsumeikan University,
1-1-1 Noji-Higashi, Kusatu-shi, Shiga-ken, 525-8577, Japan.
Tel: +81-77-561-2868.
Fax: +81-77-561-5203.

Abstract

The reflectance of fabric surface is commonly represented by a 4D bidirectional reflectance distribution function (BRDF). To generate the BRDF from measured data by a gonioreflectometer with 2 degrees of freedom of the light source and 2 degrees of freedom of the observing direction, it requires an enormous amount of measurements. In this paper, we propose an efficient image-based method for rendering the anisotropic BRDF of woven fabrics based on the micro facet surface geometry determined by the cross-sectional shape of fibers, twist of yarns, and type of weave. At first, we examine the relationship between the reflectance properties and the micro facet surface geometry of a type of woven fabric such as silk-like synthesized fabric. Next, we develop an image-based method for generating the BRDF of woven fabrics from measurement of the reflectances caused by the incident light only in the direction perpendicular to the fabric's surface. The simulation results on arbitrarily colored dresses show the performance of the proposed approach.

Categories and Subject Descriptors (according to ACM CCS): I.3.7 [Computer Graphics]: Color, shading, shadowing, and texture

1. Introduction

One of the most challenging problems in computer graphics and computer vision is modeling of deformable objects with anisotropic reflection properties such as woven fabrics. Researches on cloth simulation in CG started at late 1980th. First, wrinkles and drapes generation had been attempted by modeling dynamic behavior of fabric [VCT95], [SNI94], [HR96], [SNI94]. Then, the anisotropic reflection of fabric had been studied based on its bidirectional characteristics and various models such as the anisotropic extension of Phong model had proposed [AS00], [Kaj85], [PF90], [War92], [War94]. The reflection characteristics of a fabric surface can be described by a bidirectional reflectance distribution function (BRDF). Several methods had been proposed to generate a BRDF based on the micro facet geometry of a fabric surface [APS00], [YSY*89], where the complex luster and texture of satin or velvet was generated by modeling the micro facet geometric structure of a fabric surface.

An image-based anisotropic rendering method to obtain a BRDF based on Ward's Gaussian reflectance model [War92] was also reported [KMG96], however, anisotropic reflection was not reconstructed with high accuracy. Recently, an image-based method was proposed using newly developed optical gyro measuring machine (OGM) of omni direction type [TSM*02]. However, it requires enormous amount of data to obtain a high resolution BRDF.

In this paper, we propose an efficient image-based method for rendering the anisotropic BRDF of woven fabrics based on the micro facet surface geometry determined by the cross-sectional shape of fibers, twist of yarns, and type of weave. At first, we consider the relationship between the reflectance properties and the micro facet surface geometry of a type of woven fabric such as silk-like synthesized fabric. Next, we develop an image-based method for generating the BRDF of woven fabrics from measurement of the reflectances caused by the incident light only in the direction perpendicular to

the fabric's surface. The simulation results on arbitrarily colored dress show the performance of the proposed approach.

The remainder of this paper is organized as follows. Section 2 reviews the concept, definition of BRDF, and the geometry structure of the fiber which is an essential material to make up fabric; these contents are fundamental for presenting subsequent sections. Section 3 presents the proposed method and its analysis. Section 4 shows the experiment results. Finally, section 5 is devoted for conclusions.

2. Preliminaries

2.1. Bidirectional Reflectance Distribution Function

A bidirectional reflectance distribution function (BRDF) is a concept which describes how much light is reflected when light makes contact with a certain material. It is a function that relates the intensive of reflected light in a given viewing direction to the intensity of light incident from a given direction.
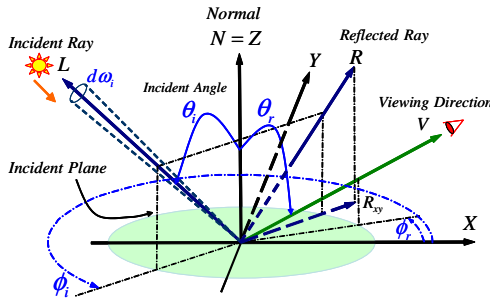

Figure 1: *Geometry of BRDF.*

A BRDF is defined in the spherical coordinate system (see Fig. 1) as the ratio of reflected radiance (W/m^2sr) in a particular direction (θ_r, ϕ_r) to the incident irradiance (W/m^2) from a direction (θ_i, ϕ_i); it is the function as follows:

$$\rho_{bd} = \frac{L_r(\theta_r, \phi_r)}{L_i(\theta_i, \phi_i)\cos(\theta_i)d\omega_i}, \qquad (1)$$

where $L_i(\theta_i, \phi_i)$ (equals to $\|\mathbf{L}\|$ in Fig. 1) is radiance coming in from a differential region of a solid angle $d\omega$ in the direction $\hat{\mathbf{L}} = (\theta_i, \phi_i)$; $L_r(\theta_r, \phi_r)$ is radiance in the direction of a viewpoint $\hat{\mathbf{V}} = (\theta_r, \phi_r)$. In this paper, $\mathbf{X}$, $\mathbf{Y}$ and $\mathbf{N}$ are the vectors representing the directions of weft, warp and normal of fabric. Besides, $\mathbf{R}$ is a vector of the reflected ray in the specular direction; $\mathbf{R_{xy}}$ is the projection of a reflected ray in the incident plane to the $\mathbf{XY}$ plane.

The BRDFs used in computer graphics can be either computed from analytical models or captured directly. The characteristics of a BRDF will determine what type of material the object is composed of. The characteristics which

are commonly concerned much are isotropic and anisotropic properties. The isotropic material has a BRDF that is independent of rotation about the normal. Therefore, with the method of direct measurement of a BRDF, only one sample in the direction ϕ_i is needed. Whereas, since an anisotropic material reflects light differently at different angles of rotation, multiple ϕ_i directions must be sampled.

In the next section, we present the surface structure of satin with its anisotropic properties. The analysis of results of measuring BRDF on satin to propose the method for rendering the anisotropic BRDF is presented in section 3.

2.2. Micro Facet Geometry of Fabrics

Figure 2: *The cross-sectional shape of synthetic fibers.*
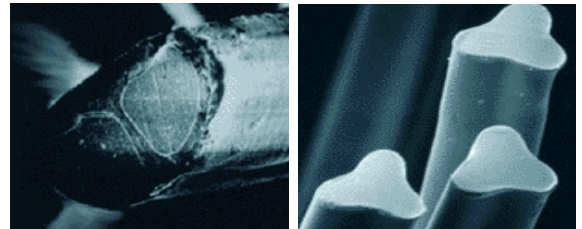
(a) Natural silk fiber.   (b) Polyester fiber.

Figure 3: *Cross-sections of natural and synthesized silk.*

Synthetic fibers have various cross-sectional shapes to reproduce luster and texture of natural fibers as shown in Fig. 2. A silk fiber is made of two fibroins and sericin, which covers these fibroins as in Fig. 3(a). Refinement after woven into fabric eliminates sericin to give the luster of silk. The silk-like synthetic fiber such as polyester has a triangular cross-sectional shape, as in Fig. 3(b), since the cross-sectional shapes of the fibroin is rounded and flattened triangle.

To develop the method for rendering the anisotropic BRDF of woven fabrics, we choose polyester satin of filament yarns as our objective fabric. In polyester satin, the cross-section shape of fibers is a dominant factor to determine the micro facet geometry of the objective fabric. This is because that the filament fiber of silk-like polyester is un-twisted and the ratio of a warp to a weft of the satin is large. Figure 4 shows the weave and the cross-section shape of fibers of our polyester satin. These characteristics of the
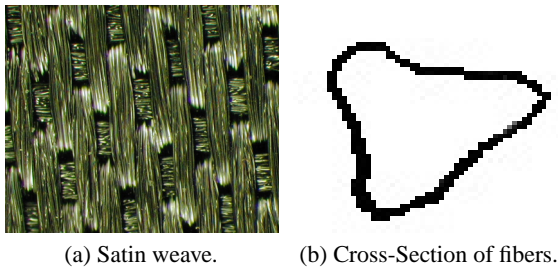
(a) Satin weave.   (b) Cross-Section of fibers.

Figure 4: *Polyester satin and cross-section of its fiber.*

satin give advantages to analyze and model the mutual relation between the cross-sectional shape of fibers, the structure of weave and reflection characteristics in the micro facet geometry.

Due to the fact that the surface of the polyester satin is considered as consisting of only warp yarns, it is necessary to investigate the reflectance distribution on a yarn. A Yarn is an assemblage of twisted fibers; the shape of the yarn can be supposed as a flattered triangular column. In such shape, the reflectance distributions of light arriving from a source at infinite distance toward the yarn in crosswise, bias and lengthwise directions are anticipated as in Fig. 5. In case of an incident ray coming from the crosswise direction, reflection rays lay in only the surface of the normal of fabric and the incident ray; in case of incident rays coming from a bias direction, the distribution of reflection rays is asymmetry with the incident plane; and in case of the lengthwise direction, the distribution is symmetry. It is obvious that reflection properties have the strong relationships with the micro facet surface geometry of a fabric.
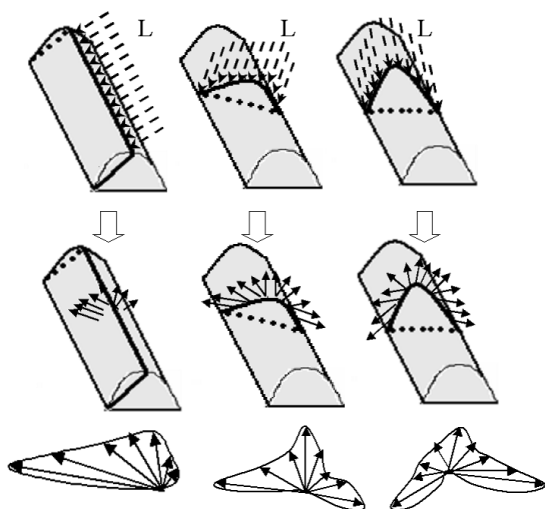

Figure 5: *Estimation of reflectance distributions of a yarn.*

Figure 5 shows the estimation of reflectance distributions on the surface of a warp yarn. In the upper part, vectors L are light vectors which come from the crosswise direction or the direction of a weft in a fabric (left), a bias direction (center) and the lengthwise direction or the warp direction (right). The middle part illustrates reflected rays on the surface of a warp yarn. The below part demonstrates our estimation of reflectance distributions.

In the next section, through measuring reflectance distributions directly to develop the method for rendering a BRDF, we also verify this prediction.

3. Proposed Method For Rendering the Anisotropic BRDF of Woven Fabrics

In this section, we show a data-driven method for rendering the anisotropic BRDF of woven fabrics based on the observation results of measuring reflectance distributions.

As mentioned in the previous section, the reflection properties of fabric have strong relationships with the micro facet surface geometry of a fabric. By the reason that the distribution of micro facets is unvarying, it is naturally thought that the reflectance distribution under the change of the angle of an incident ray has their own principles. Hence, first, we measure reflectance distributions under the change of the angle of incident rays; next we carry out analysis to find principles; and at last, we generalize the principles to propose a method for rendering the anisotropic BRDF of the fabric with least measurement.

Reflection on a surface of material is commonly described by the dichromatic reflection model which comprises two reflection components: the diffuse reflection component and specular reflection component. The diffuse component gives information of the color of material, whereas the specular reflection component informs the illumination. Due to the fact that the reflection on the polyester satin in black used in our work can be considered as comprising only the specular component, the measured BRDF is the BRDF of the specular reflection component. We can add an optional diffuse component to build the BRDF of polyester satin in color, afterward.

3.1. Measuring Anisotropic Reflection

We carry out measuring omnidirectional reflectance distributions for incident rays in the weft, bias and warp directions. Figure 6 shows an omnidirectional optical gyro measuring machine (OGM) of 4 degrees of freedom used for capturing images of fabric in omni direction. The incident angles selected for observation are 0, 15, 30, 45, 60 and 75 degrees for each weft, bias and warp directions. We obtained total of 127,440 reflected ray data by taking images of the fabric in the weft, bias and warp directions while changing viewing angle from 0 to 87 degrees by 3 degrees in the direction of regular reflection and the opposite direction.
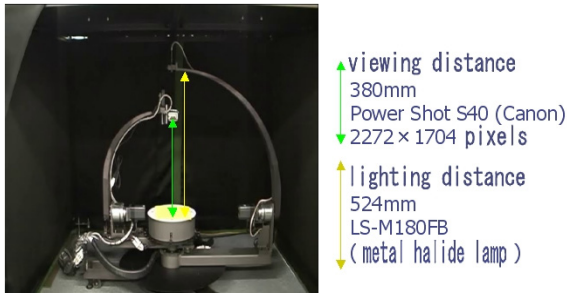
Figure 6: *Optical gyro measuring machine.*

Fig. 19, Fig. 20 and Fig. 21 show the results on the omnidirectional measurement of the fabric in the weft, bias and warp directions. The reflectance distributions corresponding to the incident angles of 0, 15, 30, 45, 60 and 75 degrees is plotted by light blue, white, green, yellow, red and blue lines, respectively.

As a result of the prediction in the section 2.2, the reflectance distributions measured by OGM as shown in Fig. 7(a), Fig. 7(b) and Fig. 7(c) is similar to the our estimation of the reflectance distributions as mentioned in the previous section (see Fig. 5).
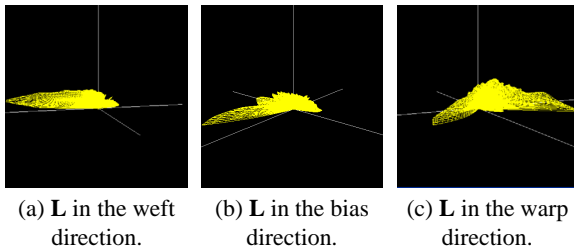

| (a) **L** in the weft direction. | (b) **L** in the bias direction. | (c) **L** in the warp direction. |

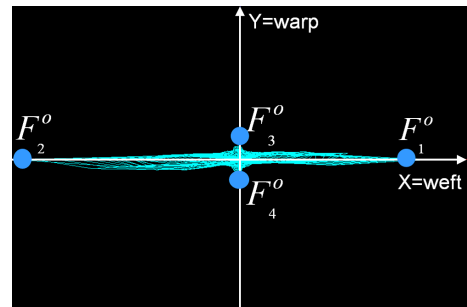**Figure 7:** *Real reflectance distributions at* $\theta_i = \frac{\pi}{4}$.

In relation to the change of a specular angle caused by the change of an incident angle, the reflectance distribution transforms likewise. Figure 19(a) and 19(c) show specular reflectance distributions concerning the change of the angle of a incident ray in the XY and YZ planes. Figure 20 and Fig. 21 show the same circumstances corresponding to incident rays in the bias and warp directions.

As it is observed, with the same azimuth angle, there are mutual relations between the reflectance distribution and the incident angle. The reflectance distribution caused by the incident ray at the angle $\theta_i = 0$ is resembling to the reflectance distributions caused by the incident ray at angles $\theta_i \neq 0$; the shape of the reflectance distribution at $\theta_i = 0$ is transformed gradually and smoothly to the shapes of reflectance distributions at $\theta_i \neq 0$. In the next section, we analysis these transformations with all the specifics.
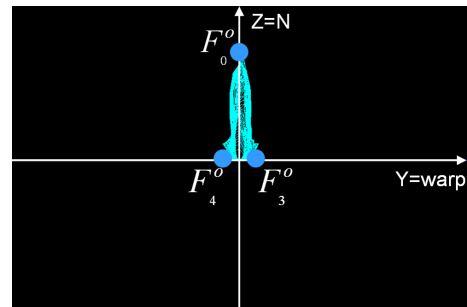
3.2. Analyzing Reflectance Distribution
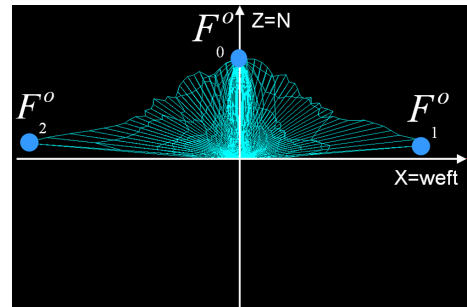
(a) Projection on XZ plane.


(b) Projection on XY plane.

(c) Projection on YZ plane.

Figure 8: *Basic anisotropic reflection distribution* ρ^o *in the spherical coordinate system.*

In this section, to inspect how the reflectance distribution of an incident ray at the angle $\theta_i = 0$ is mapped to the reflectance distributions of incident rays at angles $\theta_i \neq 0$, we analyze the relationship of reflectance distributions for the incident rays at the angles $\theta_i \neq 0$ with reference to that of the incident ray at the angle $\theta_i = 0$.

Figure 8 gives the reflectance distribution for the incident angle $\theta_i = 0$ in the spherical coordinate system; it is a result measured and then interpolated for the points which cannot be measured due to the limitations of OGM towards the reflections in incident directions. We call this reflectance distribution as basic anisotropic reflection distribution ρ^o and
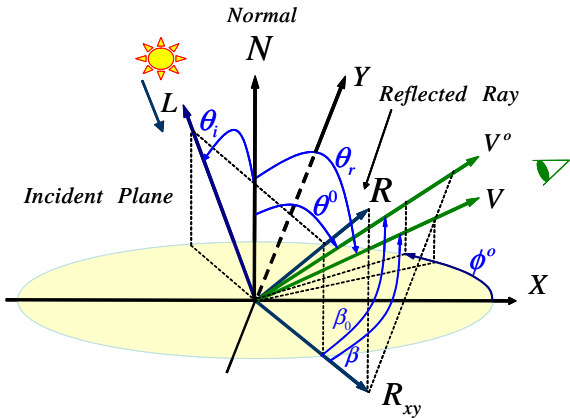
abbreviate it as BARD ρ^o. Inasmuch as the structure of a weaving fabric is symmetry to the directions of a weft and a warp, BARD ρ^o is symmetry to the **X** and the **Y** axes as well; this property can be utilized to minimize the measurement of BARD ρ^o.
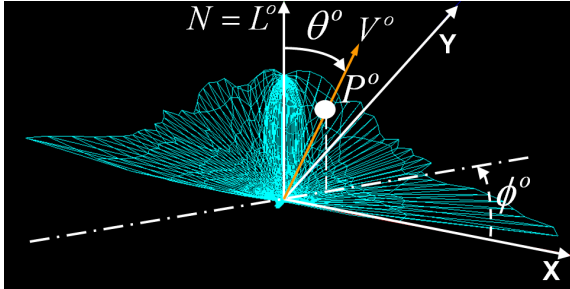
(a) Basic anisotropic reflection distribution ρ^o (BARD).
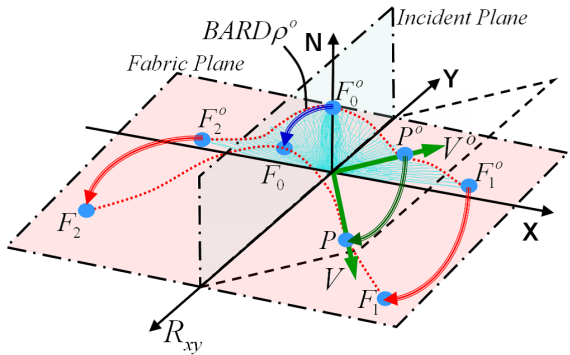
(b) Relasionship among $\mathbf{R_{xy}}$, **V** and $\mathbf{V^o}$.

(c) $\mathbf{V^o}$ in geometry of BRDF.

Figure 9: *Geometry in an anisotropic reflection.*

To examine how BARD ρ^o is gradually mapped to reflectance distributions corresponding to incident angles $\theta_i \neq 0$, we consider the feature points together with an ordinary point named P^o of BARD ρ^o. For stability, we choose the F_3^o, F_4^o which are the minima in the **Y** axis, and F_0^o, F_1^o, F_2^o which are the maxima in the **Z** and the **X** axes as the

feature points (see Fig. 8). At first, we inspect which points in the reflectance distributions of an incident ray at angles $\theta_i \neq 0$ the feature points in BARD ρ^o are corresponding to, under the change of the angle θ_i of the incident ray from 0 degree to 87 degree. Next, similarly, we inspect for the ordinary point P^o in BARD ρ^o to find the corresponding point in the reflectance distribution at an angles $\theta_i \neq 0$. We name the corresponding points with F_0^o, F_1^o, F_2^o, F_3^o, F_4^o and P^o as F_0, F_1, F_2, F_3, F_4 and P.

Physically, the points F_0^o, F_1^o, F_2^o and points F_3^o, F_4^o are the reflectance taking the maxima and the minima in the directions of **Z**, **X** and **Y** axes in BARD ρ^o caused by the incident ray at the angle $\theta_i = 0$; similarly, the points F_0, F_1, F_2 and F_3, F_4 corresponding to F_0^o, F_1^o, F_2^o and F_3^o, F_4^o are the reflectance taking the maxima and the minima under the change of the angle θ_i of an incident ray; P^o in BARD ρ^o and its corresponding P are the reflectance in distributions of at the angles $\theta_i = 0$ and $\theta_i > 0$, respectively.

For convenience, we call the unit viewpoint vector going through a point in BARD ρ^o as $\mathbf{V^o}$ and the unit viewpoint vector going through its corresponding point in reflectance distribution at $\theta_i \neq 0$ as **V**. The figure 9(a) shows the vector $\mathbf{V^o}$ with its direction (θ^o, ϕ^o) and P^o with its the radial coordinate r^o.

From the measured results in the previous section, as shown in Fig. 9(b), we reach an important conclusion that under the change of the angle θ_i of an incident ray, the change of a vector **V** corresponding to a $\mathbf{V^o}$ in BARD ρ^o takes places only in the plane composed by $\mathbf{V^o}$ and $\mathbf{R_{xy}}$, where $\mathbf{R_{xy}}$ is the projection a reflected ray in the incident plane to the **XY** plane. Besides, F_3 and F_4 are almost unchanged; this means that we always have $F_3 = F_3^o$, $F_4 = F_4^o$ under any change of the incident angle.

In Fig. 9(c), β is an angle between $\mathbf{R_{xy}}$ and **V**; and β^o is an angle between $\mathbf{R_{xy}}$ and $\mathbf{V^o}$. Note that $\mathbf{R_{xy}}$, **V** and $\mathbf{V^o}$ share a plane. In the next sections, so as to examine the relation between of P and P^o under the change of the angle of an incident ray, we inspect relation between the angles β and β^o.

Analysis of the Transformation of the Reflectances in the Incident Plane

At first, we inspect the transformation of a reflectance of the feature point F_0 in the incident plane (see Fig. 10). Table 1 shows the result comparing the change of the reflectance ρ_{F_0} ($= \rho_{bd}(\theta_s, \frac{3\pi}{2}, \theta_i, \frac{\pi}{2})$) and the reflection angle θ_s ($= \frac{\pi}{2} - \beta$) accompanying with the increase of an incident angle θ_i, in union with the increase ratio of the reflectance at F_0 toward the reflectance at F_0^o ($\rho_{F_0^o}^o = \rho_{bd}(0, \frac{3\pi}{2}, 0, \frac{\pi}{2})$) of the incident angle $\theta_i = 0$ such as: $\rho_{F_0}/\rho_{F_0^o}^o$, $1/cos\theta_i$ and $1/cos\theta_i cos\theta_s$. Figure 11 presents these relationships in a graph.

From this result, the angle of the reflection at the peak value of the reflection is similar to the incident angle; $\theta_s =$
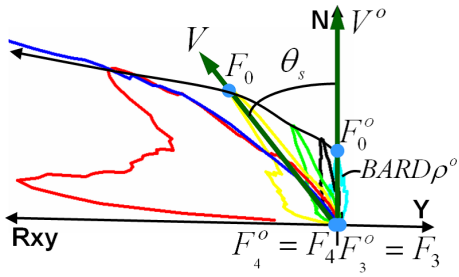
Figure 10: *Tracing F_0 in the incident plane.*

θ_i	θ_s	ρ_{F_0}	$\frac{\rho_{F_0}}{\rho^o_{F_0}}$	$\frac{1}{cos\theta_i}$	$\frac{1}{cos\theta_i cos\theta_s}$
0	0	0.213	1.000	1.000	1.000
15	14	0.301	1.409	1.035	1.072
30	29	0.356	1.670	1.155	1.333
45	45	0.434	2.033	1.414	2.000
60	61	1.033	4.841	2.000	4.000
75	76	4.354	20.403	3.861	14.93

Table 1: *Comparing the incident angle and the reflectance in the incident plane.*
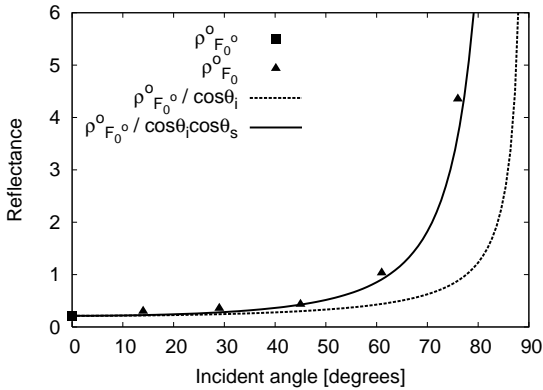

Figure 11: *Reflection in the incident plane.*

θ_i, and the increase of the reflectance at the peak value of a reflection accompanying with the increase of the angle of an incident ray is approximate $1/cos^2\theta_i$ of the reflectance of the incident ray in the angle $\theta_i = 0$. We have the expression as follows:

$$\rho_{bd}(\theta_s, \frac{3\pi}{2}, \theta_i, \frac{\pi}{2}) = \rho_{bd}(\theta_s, \frac{3\pi}{2}, 0, \frac{\pi}{2}) \frac{1}{cos^2\theta_i}. \quad (2)$$

Next, to investigate the changing of the reflectance at the points different to the feature point, we compare the re-

flectance of incident rays at angles $\theta_i > 0$ with that of the incident ray in the angle $\theta_i = 0$ in the incident plane.
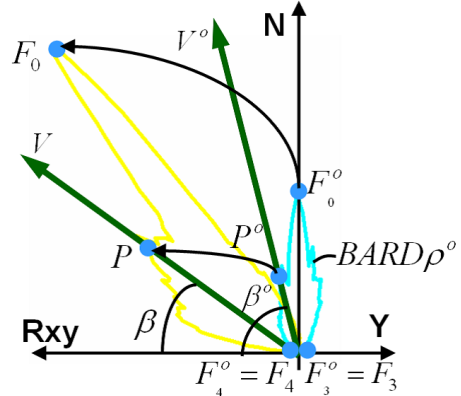

Figure 12: *Mapping reflectance distribution in the incident plane.*

In Fig. 12, F_0^o, F_3^o, F_4^o are three feature points in BARD ρ^o of the incident ray at the angle $\theta_i = 0$. F_3^o, F_4^o are the points which show the reflectance in the horizon direction of the incident plane. β^o is the angle of the vector $\mathbf{R_{xy}}$ and the viewpoint vector $\mathbf{V^o}$ going through P^o in BARD ρ^o; β is the angle between the vector $\mathbf{R_{xy}}$ and the viewpoint vector $\mathbf{V}$ going through P. Under the change of the angle of an incident ray, F_3^o, F_4^o are unchanged but F_0^o is changed to F_0.

In other words, at F_3^o, F_4^o, we have $\beta^o = \beta$; and at F_0 corresponding to F_0^o, we have $\beta^o \neq \beta$. The range from F_4^o to F_0^o in the reflectance distribution of the incident ray at the angle $\theta_i = 0$ is reducing to the range F_4 to F_0 in the reflectance distribution of the incident ray at θ_i ($\neq 0$); and the range from F_3^o to F_0^o in the reflectance distribution of the incident ray at angle $\theta_i = 0$ is magnifying to the range F_3 to F_0 in the reflectance distribution of the incident ray at θ_i. The reduction and magnification of the reflectance at two adjacent ranges of which common boundary point is F_0 is considered to be linear. Therefore, the relation of β and β^o can be expressed by the expression (3). This expression shows the relation of the point P toward the point P^o in BARD ρ^o:

$$\beta^o = \begin{cases} \frac{\pi/2}{\pi/2-\theta_s}\beta & \text{if } 0 \leq \beta \leq \pi/2 - \theta_s \\ \frac{\pi/2}{\pi/2+\theta_s}\beta + \frac{\pi}{\pi/2+\theta_s}\theta_s & \text{if } \pi/2 - \theta_s \leq \beta \leq \pi \end{cases} \quad (3)$$

Analysis of the Transformation of the Reflectances in the Fabric Plane

Similarly to the previous section, we inspect the transformation of the reflectance of the feature points due to the change of the incident angle in the fabric plane. Because F_1 and F_2 are symmetry to the **Y** axis, we focus on F_2. Table 2 shows the result comparing the change of reflectance ρ_{F_2}
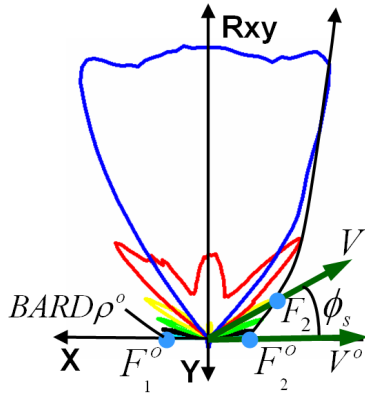
Figure 13: *Tracing F_2 in the fabric plane.*

θ_i	ϕ_s	ρ_{F_2}	$\frac{\rho_{F_2}}{\rho^o_{F_0}}$	$\frac{1}{cos\theta_i}$	$\frac{1}{cos\theta_i cos\phi_s}$
0	1	0.452	1.000	1.000	1.000
15	16	0.479	1.060	1.035	1.072
30	31	0.597	1.323	1.155	1.333
45	45	0.901	1.996	1.414	2.000
60	59	1.809	4.008	2.000	4.000
75	76	4.737	10.493	3.861	14.93

Table 2: *Comparing the incident angle and the reflections in the fabric plane.*
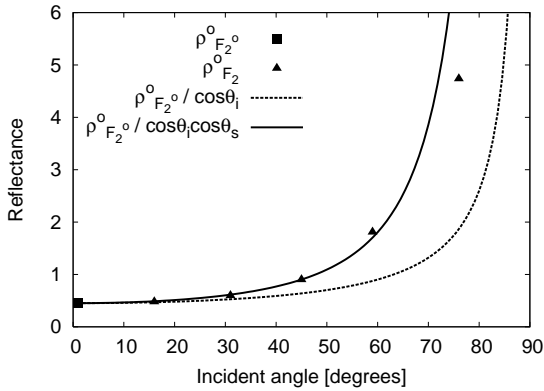

Figure 14: *Reflection in the fabric plane.*

($= \rho_{bd}(\theta_s, \phi_s, \theta_i, \frac{\pi}{2})$) and the reflection angle ϕ_s ($=\frac{\pi}{2} - \beta$) accompanying with the increase of the incident angle θ_i, in union with the increasing ratio of the reflectance at F_2 toward the reflectance at F_2^o ($\rho^o_{F_2^o} = \rho_{bd}(\theta_s, \phi_s, 0, \frac{\pi}{2})$) of the incident angle $\theta_i = 0$ such as: $\rho_{F_2}/\rho^o_{F_2^o}$, $1/cos\theta_i$ and $1/cos\theta_i cos\phi_s$.

We have the similar conclusion that the angle of the reflection at the peak value of reflection is similar to the inci-

dent angle of the incident ray: $\phi_s = \theta_i$, and the increase of the reflectance at the peak value of reflection accompanying with the increase of the incident angle is approximate $1/cos\theta_i cos\phi_s$ of the reflectance of the incident ray at the angle$\theta_i = 0$:

$$\rho_{bd}(\frac{\pi}{2}, \phi_s, \theta_i, \frac{\pi}{2}) = \rho_{bd}(\frac{\pi}{2}, \phi_s, 0, \frac{\pi}{2})\frac{1}{cos^2\theta_i}. \qquad (4)$$

Next, to investigate the change of the reflectance at the points different to the feature point, we also compare the reflectance of an ordinary point P with that of P^o in BARD ρ^o.
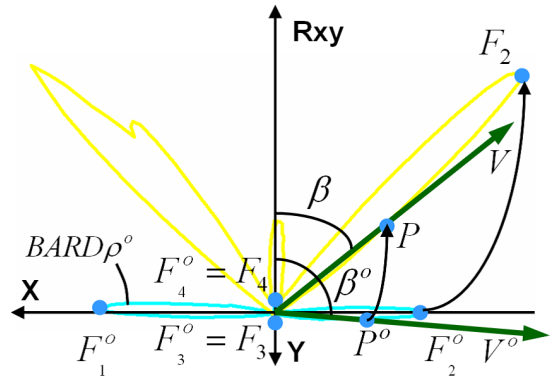

Figure 15: *Mapping reflectance distribution in the fabric plane.*

In Fig. 15, F_2^o, F_3^o, F_4^o are three feature points in BARD ρ^o of the incident ray at the angle $\theta_i = 0$. F_2, F_3, F_4 are the corresponding points explained in above. Under the change of the angle of an incident ray, F_3, F_4 are unchanged but F_2 is changed. The relation of the point P toward the point P^o in BARD ρ^o is expressed by the following expression:

$$\beta^o = \begin{cases} \frac{\pi/2}{\pi/2-\phi_s}\beta & \text{if } 0 \le \beta \le \pi/2 - \phi_s \\ \frac{\pi/2}{\pi/2+\phi_s}\beta + \frac{\pi}{\pi/2+\phi_s}\phi_s & \text{if } \pi/2 - \phi_s \le \beta \le \pi \end{cases} \qquad (5)$$

Analysis of the Transformation of the Reflectances in an Inclined Plane

From measured results, we see that the feature point F_0 of the reflection of the incident ray at an angle θ_i as shown in Fig. 10 moves in a way that the relation $\theta_s = \theta_i$ is always satisfied. The motion of the viewpoint vector **V** of F_0 has tendency to approach $\mathbf{R_{xy}}$; and the reflectance increases in ratio to $1/cos^2\theta_i$. Similarly, the trajectory of the feature point F_1, F_2 according to the increment of the incident angle θ_i as showed in Fig. 15 changes linearly in a plane in the directions which comes near to $\mathbf{R_{xy}}$; the reflectance increases in ratio to $1/cos^2\theta_i$.

Generally, we predict that the reflectance of the points which are in the inclined plane as shown in Fig. 9(b) also have the same characteristic under the change of an incident angle. The relation between the reflectance of a feature point F^o and ordinary points P^o on BARD ρ^o and the corresponding points F, P is supposed to be satisfied the following expressions:

$$\rho_{bd}(\theta_s,\phi_s,\theta_i,\phi_i) = \rho_{bd}(\theta_s,\phi_s,0,\phi_i)\frac{1}{cos^2\theta_i}, \qquad (6)$$

$$\beta^o = \begin{cases} \frac{\pi/2}{\pi/2-\theta_i}\beta & \text{if } 0 \leq \beta \leq \pi/2-\theta_i \\ \frac{\pi/2}{\pi/2+\theta_i}\beta + \frac{\pi}{\pi/2+\theta_i}\theta_i & \text{if } \pi/2-\theta_i \leq \beta \leq \pi \end{cases} \qquad (7)$$
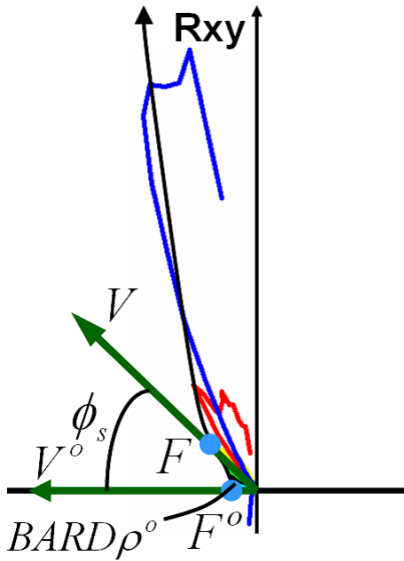

Figure 16: *Tracing F in an inclined plane.*

θ_i	ϕ_s	ρ_F	$\frac{\rho_F}{\rho_{F^o}^o}$	$\frac{1}{cos\theta_i}$	$\frac{1}{cos^2\theta_i}$
0	2	0.266	1.000	1.000	1.000
15	18	0.259	0.975	1.035	1.072
30	32	0.346	1.301	1.155	1.333
45	46	0.555	2.087	1.414	2.000
60	58	1.267	4.765	2.000	4.000
75	75	4.531	17.045	3.861	14.93

Table 3: *Comparing the incident angle and the reflections in an inclined plane.*

From measured reflectance distributions, we see that this relation is true for any feature points F^o and ordinary points P^o on BARD ρ^o in a direction of $\mathbf{V^o}$ and the corresponding
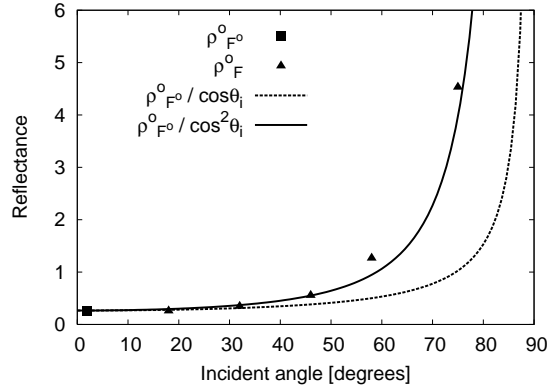

Figure 17: *Reflection in the inclined plane.*

points F, P inside the plane which is consisted of the vector $\mathbf{V^o}$ and the vector $\mathbf{R_{xy}}$. Figure 16 shows a reflectance distribution in an inclined plane composed by the vector $\mathbf{R_{xy}}$ and vector $\mathbf{V^o}$ which is the viewpoint vector of at a vector F^o laying between F_0^o and F_1^o in BARD ρ^o and in the plane of vectors $\mathbf{N}$ and $\mathbf{X}$ (refer Fig. 9(b)). Table 3 and the graph in Fig. 17 also shows the result comparing the change of reflectance ρ_F ($= \rho_{bd}(\theta_s,\phi_s,\theta_i,\frac{\pi}{2})$) and the reflection angle ϕ_s ($=\frac{\pi}{2}-\beta$) accompanying with the increase of the incident angle θ_i, in union with the increasing ratio of the reflectance F toward the reflectance F^o ($\rho_{F^o}^o = \rho_{bd}(\frac{\pi}{4},0,0,\frac{\pi}{2})$). We also acquire the result similar to (6) for the feature points F, F^o and then (7) for the ordinary points P, P^o.

Thus, in most situations, in most situations, the expressions (6) and (7) can be used for calculating the reflectances of incident ray at the angles $\theta_i > 0$ from the reflectance at the angle $\theta_i = 0$.

3.3. Generating Anisotropic BRDF

From the results of the prior sections, it follows that we can generate the reflectance distribution at any directions of a incident ray from the measured BARD ρ^o for the incident ray at the angle ($\theta_i = 0$); and the BRDF can be obtained by the following expression:
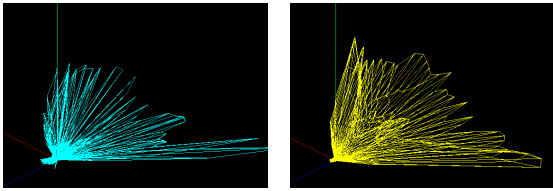
$$\rho_{bd}(\theta_r,\phi_r,\theta_i,\phi_i) = \frac{\rho_d}{\pi} + \frac{1}{cos^2\theta_i}\rho^o(\theta^o,\phi^o), \qquad (8)$$

where (θ_r,ϕ_r) is the reflection direction or the viewing direction, (θ_i,ϕ_i) is an incident ray direction, ρ_d is diffuse reflectance, $\rho^o(\theta^o,\phi^o)$ is BARD in the direction (θ^o,ϕ^o) of $\mathbf{V^o}$. Figure 9(b) gives an illustration of this expression. Because $\mathbf{V^o}$ lays in the plane of the vectors $\mathbf{R_{xy}}$ and $\mathbf{V}$, we have:

$$\theta^o = \frac{\pi}{2} - \frac{\beta^o}{\beta}(\frac{\pi}{2}-\theta_r), \qquad (9)$$

$$\phi^o = \frac{\beta^o \phi_r}{\beta}. \qquad (10)$$

4. Experimental Results

(a) Simulated reflectance distribution.

(b) Real reflectance distribution.

Figure 18: *Simulated v.s. real reflectance distribution of a satin cloth.*

We evaluated our method by comparing the calculated results of reflection on the satin cloth with the results measured actually by OGM. Figure 18(a) and (b) show the comparison result of reflectance distribution by the incident ray in the direction ($\theta_i = \frac{\pi}{4}, \phi_i = \frac{\pi}{2}$). Figure 22 shows the simulation results on arbitrarily colored satin dress using our proposed method.

5. Conclusion

We have proposed an efficient image-based method for rendering the anisotropic reflection of woven fabrics based the micro facet surface geometry determined from the cross-section shape of fibers, the twist of yarns, and the type of weave. The experimental and simulation results on the arbitrarily colored satin dress demonstrated the performance of our proposed method.

References

[APS00] ASHIKHMIN M., PREMOZE S., SHIRLEY P.: A microfacet-based brdf generator. In *Proc. SIG-GRAPH 2000* (July 2000), pp. 65–74.

[AS00] ASHIKHMIN M., SHIRLEY P.: An anisotropic phong brdf model. *Journal of Graphics Tools 5*, 2 (2000), 25–32.

[BW98] BARAFF D., WITKIN A.: Large steps in cloth simulation. In *Proc. SIGGRAPH '98* (1998), pp. 43–54.

[HR96] HING N. N., RICHARD L. G.: Computer graphics techniques for modeling cloth. *IEEE Computer Graphics and Applications 16*, 5 (Sept. 1996), 28–41.

[Kaj85] KAJIYA J. T.: Anisotropic reflection models. *Computer Graphics 19*, 3 (July 1985), 15–21.

[KMG96] KARNER K. F., MAYER H., GERVAUTZ M.: An image based measurement system for anisotropic reflection. In *Proc. EUROGRAPH-ICS '96* (1996), vol. 15(3), pp. 119–128.

[NRH97] NICODEMUS F. E., RICHMOND J. C., HSIA J. J.: *Geometric Considerations and Nomenclature for Reflectance*. U.S. Dept. of Commerce National Bureau of Standards, Oct. 1997.

[PF90] POULIN P., FOURNIER A.: A model for anisotropic reflection. *Computer Graphics 24*, 4 (Aug. 1990), 273–282.

[SNI94] SAKAGUCHI Y., NIMOU M., IKEDA K.: Party. an numerical calculation method for a dynamically deformable cloth model. *Trans. of IEICE J77-D-2 5* (1994), 912–921. (In Japanese).

[TSM*02] TAKEMURA S., SAKAGUCHI Y., MITSUI S., KUNIMATSU A., YAMAUCHI Y., CHIHARA K.: Measurement and visualization of anisotropic reflectance. In *Proc. of SICE 2002* (2002).

[VCT95] VOLINO P., COURCHESNE M., THALMANN N. M.: Versatile and efficient techniques for simulating cloth and other deformable objects. In *Proc. SIGGRAPH '95* (Aug. 1995), pp. 137–144.

[War92] WARD G. J.: Measuring and modeling anisotropic reflection. In *Proc. SIGGRAPH '92* (July 1992), vol. 26(2), pp. 255–272.

[War94] WARD G. J.: The radiance lighting simulation and rendering system. In *Proc. Computer Graphics* (July 1994), pp. 459–472.

[YSY*89] YASUDA T., SUZUKI K., YOKOI S., TORIWAKI J., INAGAKI K.: A reflection model of cloth with anisotropy. In *Proc. the fifth NICOGRAPH* (1989), pp. 215–223.